

N -slit interference: fractals in near-field region, bohmian trajectories.

Valeriy I. Sbitnev*

*B.P.Konstantinov St.-Petersburg Nuclear Physics Institute,
Russ. Ac. Sci., Gatchina, Leningrad district, 188350, Russia.*

(Dated: October 29, 2018)

Scattering cold particles on an N -slit grating is shown to reproduce an interference pattern, that manifests itself in the near-field region as the fractal Talbot carpet. In the far-field region the pattern is transformed to an ordinary diffraction, where principal beams are partitioned from each other by $(N - 2)$ weak ones. A probability density plot of the wave function, to be represented by a gaussian wavepacket, is calculated both in the near-field region and in the far-field one. Bohmian (geodesic) trajectories, to be calculated by a guidance equation, are superimposed on the probability density plot well enough. It means, that a particle, moving from a source to a detector, passes across the grating along a single bohmian trajectory through-passing one and only one slit.

Keywords: Gaussian wavepacket, neutron scattering, guidance equation, bohmian trajectory, near-field interference, far-field diffraction, Talbot carpet, fractal

I. INTRODUCTION.

Wave interference is a most impressive phenomenon be it induced by waves on water, acoustic waves, or electromagnetic ones - radio-waves, light waves, γ -radiation. Quantum-mechanical experiments dealing with interference phenomena [1] display interesting interference phenomena. They involve self-affine fractal quantum evolution of the probability densities and quantum revivals [2, 3, 4, 5, 6]. There is a special interest to the phenomena from the side of quantum computation and communication [7, 8, 9].

Most fantastic interference effects are disclosed in near-field region, i.e., in the vicinity of an interference grating. In this region complex wave interference shows very exotic patterns named in literature as the Talbot carpets [2, 3, 4]. They disclose fractal-like self-similar structures. Henry Fox Talbot was first who observed in 1836 such an effect in a near-field region[32]. Fig. 1, for example, demonstrates the optical Talbot carpet for monochromatic light to be scattered on 4-slit grating. A significant parameter in this optical pattern is the Talbot Length

$$z_T = \frac{2d^2}{\lambda}, \quad (1)$$

where d is the period of the diffraction grating

and λ is the wavelength of the light incident on the grating. We will deal with this parameter often enough at representations of interference patterns in near-field regions. Instead of monochromatic light scattering, however, we will simulate here particles (cold neutrons) scattering on nanoscale gratings (the period d is multiple of the particle wavelength).

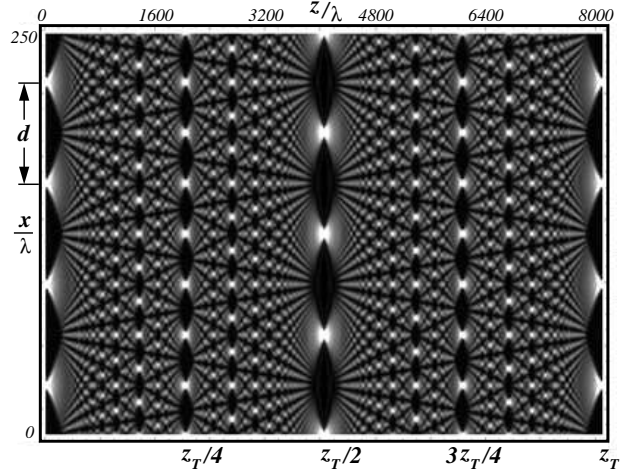


FIG. 1: The optical Talbot effect for monochromatic light, shown as a "Talbot Carpet". The figure has been captured from http://en.wikipedia.org/wiki/Talbot_effect.

On the other hand, as a distance from the slit grating to a detector increases the exotic near-field interference transforms to a diffraction pattern observed in the far-field region. Beautiful magnificence of the fractal structures disappears. Instead of it divergent rays from the slit source come into being. Intensity of these rays is de-

*Electronic address: valeriy.sbitnev@gmail.com

scribed by a well-known formula [10]

$$I(\zeta) = I_0(\zeta) \cdot \frac{\sin^2 \frac{N\zeta}{2}}{\sin^2 \frac{\zeta}{2}} \quad (2)$$

Function $I_0(\zeta)$ is an envelope describing diffraction on a single slit and

$$\zeta = \frac{2\pi}{\lambda} d \sin(\theta)$$

is a phase shift of the waves emitted from two nearest slits, see Fig. 2. Observe that Eq. (2) is quite common formula. For example, it describes also revolution of spin of neutrons flying through an N -periodic magnetic field [11].

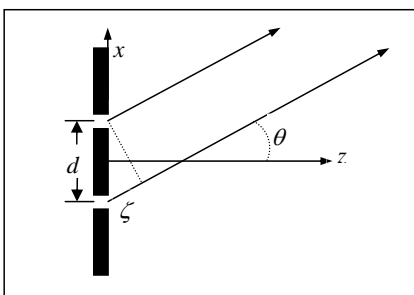


FIG. 2: Diffraction from two slits in far-field region: d is distance between the slits, θ is deflection angle with respect to axis z , and ζ is phase shift of wave rays emitted from the slits.

Most striking observation in Fig. 1 is existence of fractal structures, sizes of which are smaller than distance between slits. As was mentioned above, emergence of the fractal structures have been studied by Berry *et al.* [4], Amanatidis *et al.* [5], Sanz [6]. Sanz, in particular, has devoted the studies whether one can depict by the Bohmian trajectories the quantum fractal structures. The authors note that universal fractal features of quantum theory might be useful in the field of quantum information, for creating efficient quantum algorithms.

As was mentioned, interference effects in the near-field regions can be important with the point of view of quantum computing perspective. Theoretical study of the near-field interference by means of preparation of quantum mechanical models is the first step for an understanding of the quantum computing perspective. Gaussian

wavepacket [12, 13] is a simplest model for studying N -slit grating interference. Sec. II deals with the Gaussian wavepacket and its Fourier transforms that give rise to emergence of complex, time-dependent, variance. In Sec. III we simulate interference by radiation of the Gaussian wavepackets from the N -slit grating. Their dispersion in the near-field region produces an interference pattern that manifests itself in a fractal organization of probability density of the wave function. As the detector is shifted in the far-field region the interference pattern transforms to diffraction pattern described by Eq. (2). In that region fractality disappears. Instead of this, principal maxima of radiation come into being. And they are partitioned by $(N - 2)$ subsidiary maxima. Next, the problem is to understand, how does a particle pass through the N -slit grating up to a detector. David Bohm had revealed that the particle travels along a single optimal trajectory [14, 15], which is named in literature the bohmian trajectory. This approach together with calculation of trajectories is discussed in Sec. IV. Emergence and development of the fractal Talbot patterns are considered in Sec. V at the slit grating containing many slits and at varying the period d of the grating. Comparison of classical trajectories and bohmian is given in Sec. VI, concluding section. In this section we discuss the bohmian trajectories passing through a slit up to the detector, and waviness of the bohmian trajectories caused by exchange of virtual particles with vacuum that is tuned by de Broglie pilot-wave.

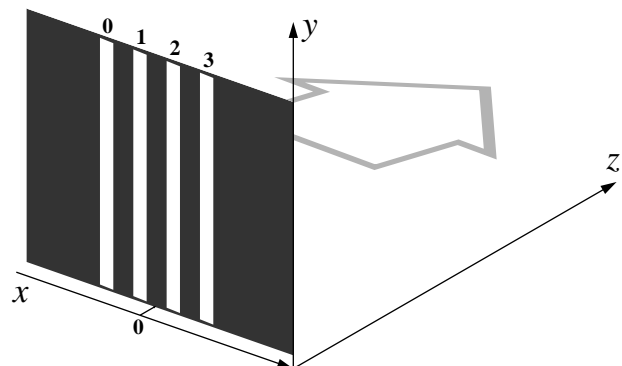


FIG. 3: Interference experiment in a cylindrical geometry - the grating is placed in the plane (x, y) and slits go along the axis y . Gray arrow points direction of wave radiation.

II. GAUSSIAN WAVEPACKET AND ITS FOURIER TRANSFORMS.

As seen in Fig. 2, Eq. (2) results from computation of interference of cylindrical waves divergent from the slits. The waves in the vicinity of the slits are no cylindrical, in general. They have a complex form when transforming from a plane wave to cylindrical one. For the sake of simplicity, we suppose that slit borders are fuzzy under Gauss distribution, and a wave from the slit is approximated by the Gaussian wavepacket [12, 16]

$$\varphi_0(x) = \sqrt[4]{\frac{1}{2\pi\sigma^2}} \exp\left\{-\frac{(x-x_0)^2}{4\sigma^2}\right\}. \quad (3)$$

$$\begin{aligned} F_x[\varphi_0(x)](k) &= \sqrt[4]{\frac{1}{2\pi\sigma^2}} \int_{-\infty}^{\infty} \exp\left\{-\frac{(x-x_0)^2}{4\sigma^2}\right\} \exp\{-2\pi\mathbf{i}kx\} dx \\ &= \sqrt[4]{8\pi\sigma^2} \exp\{-\pi^2 4\sigma^2 k^2\} \exp\{-2\pi\mathbf{i}kx_0\} = \Phi_0(k). \end{aligned} \quad (4)$$

The function $\Phi_0(k)$ is seen to be a harmonic wave $\exp\{-2\pi\mathbf{i}kx_0\}$ having an amplitude

$$A(k) = \sqrt[4]{8\pi\sigma^2} \exp\{-\pi^2 4\sigma^2 k^2\}. \quad (5)$$

As we move off from the slit, the wave components $\Phi_0(k)$ spread along axis x differently for different k . Let the dispersed wave component be $\Phi_0(k) \exp\{-\mathbf{i}2\pi k \cdot \pi x\}$. Additional factor π scales the dispersion along axis x . Observe that $x = vt$ and a speed of the shift along

Observe that $\varphi_0^2(x) = p(x)$ is the probability density distribution that has a mean x_0 and variance $\sigma^2 \geq 0$.

We believe that in the immediate neighborhood on each slit, see Fig. 3, a wave field is described by the Gaussian wavepacket (3). It rely on assumption that edges of the slits are not ideal, but rather fuzzy.

Observe that the wavepacket (3) disperses as it moves away from the slit to a region pointed out by grey arrow in Fig. 3. Let us express this wavepacket by superposition of harmonic waves $\exp\{-2\pi\mathbf{i}kx_0\}$ with wave number k ranging from $-\infty$ to ∞ . To that end, we execute the Fourier transform

axis x is $v = \hbar k/m$. Here \hbar is the reduced Planck constant, m is a particle mass. As far as $2\pi k \cdot k = (2\pi k)^2/2\pi$, a shifted wave component is

$$\Phi_0(k) \exp\left\{-\mathbf{i}(2\pi k)^2 \frac{\hbar}{2m} \cdot t\right\}. \quad (6)$$

Let us now execute the inverse Fourier transform of the function (6)

$$\begin{aligned} F_k \left[\Phi_0(k) \exp\left\{-\mathbf{i}(2\pi k)^2 \frac{\hbar}{2m} \cdot t\right\} \right] (x) \\ &= \sqrt[4]{8\pi\sigma^2} \int_{-\infty}^{\infty} \exp\{-\pi^2 4\sigma^2 k^2\} \exp\left\{-\mathbf{i}(2\pi k)^2 \frac{\hbar}{2m} \cdot t\right\} \exp\{2\pi\mathbf{i}k(x-x_0)\} dk \\ &= \sqrt[4]{\frac{2}{4\pi\sigma_t^2}} \exp\left\{-\frac{(x-x_0)^2}{4\sigma\sigma_t}\right\} = \phi(x, x_0, t). \end{aligned} \quad (7)$$

Here

$$\sigma_t = \sigma \left(1 + \mathbf{i} \frac{\hbar}{2m} t \cdot \sigma^{-2} \right) \quad (8)$$

is a complex time-dependent spreading. It

should be noted, that it is a complex variable of time t . Getting ahead, we can say that this complex variable [12, 13] determines fractal pattern in the near-field region. Observe that at $t = 0$ we have $\sigma_{t=0} = \sigma$ and the function (7) comes to $\phi_0(x)$.

III. RADIATION FROM N -SLIT GRATING.

The function (7) is not yet a wave function since it contains no a term describing its translation forward the region, as shown by grey arrow in Fig. 3. The term describing such a translation along axis z is represented by a factor $\exp\{\mathbf{i}\omega t - \mathbf{i}k_z z\}$. Here $E = \hbar\omega$ is a particle energy and $p_z = \hbar k_z$ is its momentum along axis z . The wave function, in such a case, reads

$$\Psi(x, x_0, z) = \phi(x, x_0, t) \exp\{\mathbf{i}\omega t - \mathbf{i}k_z z\} \quad (9)$$

$$= \sqrt[4]{\frac{2}{4\pi\sigma_t^2}} \exp\left\{-\frac{(x-x_0)^2}{4\sigma\sigma_t}\right\} \exp\{\mathbf{i}\omega t - \mathbf{i}k_z z\}.$$

A velocity along axis z is $v_z = p_z/m = \hbar k_z/m$. So, we can express time t in the function (9) via variable z/v_z . Therefore, arguments in the function $\Psi(x, x_0, z)$ do not contain t .

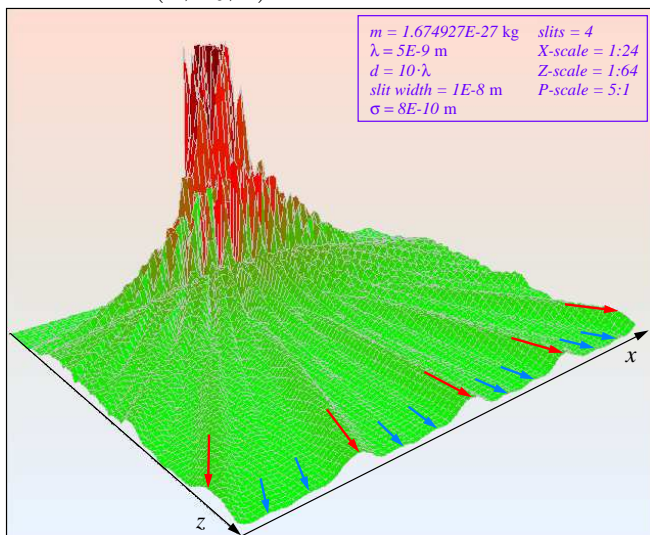


FIG. 4: Diffraction pattern in a transient region, $(x; z) \in ((0 \dots 1.4 \times 10^{-6}); (5 \times 10^{-8} \dots 3.8 \times 10^{-6}))$ m, from near-field to far-field ones. Red arrows point out to directions of radiation along the principal peaks. Blue arrows point out to directions of weak radiation along the subsidiary maxima.

Putting the frame of axis x in center of the slit grating, containing $(N + 1)$ slits, $(n =$

$0, 1, 2, \dots, N)$, as shown in Fig. 3, we find that position of n^{th} slit is $x_0 = (n - N/2)d$. Here distance d is period of the grating. Superposition of the waves (9) emitted by all $(N + 1)$ slits reads

$$|\Psi(x, z)\rangle = \frac{1}{N + 1} \sum_{n=0}^N \Psi\left(x, \left(n - \frac{N}{2}\right)d, z\right). \quad (10)$$

Probability density

$$p(x, z) = \langle \Psi(x, z) | \Psi(x, z) \rangle \quad (11)$$

is an observable. Fig. 4 shows the probability density $p(x, z)$ which is calculated within a transient region from the near-field region to the far-field ones. The grating contains four slits. It should be noted, that coordinate z in this figure begins from a value that is slightly more than zero. The whole point is that the wave function at $z = 0$ has singularities located on the slits.

Here we have simulated neutron scattering on the slits, with the neutrons having a wavelength $\lambda = 5\text{nm}$. Kinetic energy of the neutrons is about 5.25×10^{-24} J. It means, that the neutrons are very cold [33], i.e., temperature of the neutrons is about $T = E/kB \approx 0.38$ K. Here $kB \approx 1.38 \times 10^{-23}$ JK $^{-1}$ is the Boltzmann constant.

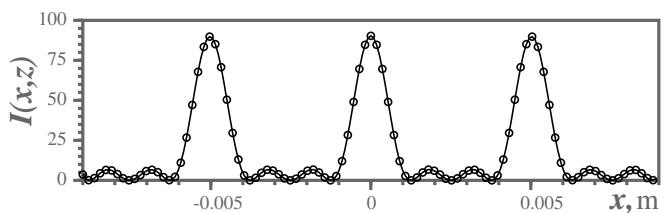


FIG. 5: Diffraction in the far-field region, $z = 0.004$ m. Cross-section of the diffraction pattern (see previous figure) is displayed by circles. Solid curve shows the same cross-section calculated by the diffraction formula (2) with parameters ζ and I_0 defined in Eqs. (12) and (13).

Fig. 4 demonstrates diffraction pattern in a transition region from the near-field region to the far-field one. Red arrows point out to the principal maxima. And blue arrows point out to the subsidiary maxima. Alternation of the principal maxima and subsidiary ones is described by Eq. (2). Parameters ζ and I_0 , in this case, have the following forms [10]

$$\zeta(x, z) = xd \frac{m\hbar(z/v_z)}{D(z)} \quad (12)$$

and

$$I_0(x, z) = \sqrt{\frac{1}{\pi}} \frac{m\sigma}{\sqrt{D(z)}} \exp\left\{-\frac{2m^2\sigma^2 x^2}{D(z)}\right\}, \quad (13)$$

where denominator $D(z)$ is as follows

$$D(z) = m^2\sigma^4 + \hbar^2(z/v_z)^2/4. \quad (14)$$

Here $(z/v_z) = t$ is a flight time along the path length z . Diffraction curve (2), at substituting terms ζ and I_0 by functions (12)-(13), has been calculated in the far-field region, $z = 0.004$ m, is shown in Fig. 5. Circles in this figure relate to results simulated by means of the Gaussian wavepacket.

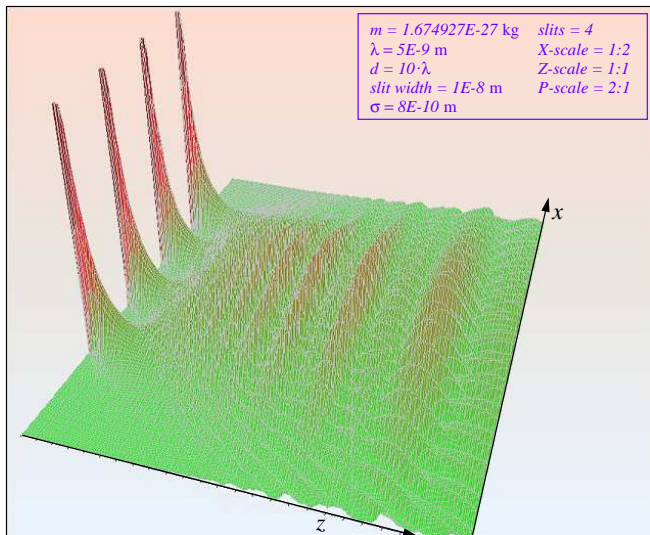


FIG. 6: Diffraction pattern in the near-field region, $(x, z) \in ((0 \dots 3 \times 10^{-7}); (8 \times 10^{-10} \dots 2 \times 10^{-7}))$ m. Ripples of the probability density lengthen as distance to the N-slit sources is increased.

Turn back to Fig. 4. In order to show the diffraction pattern in the far-field region, we have coarsen resolution of the probability density distribution. For this reason, we see a rough pile-up of maxima in the near-field region. Fig. 6 shows the same pattern at more detailed resolution in the near-field region. One can see, the probability density distribution increases catastrophically nearby the slits. At some distance from the slits, their radiations are superimposed with each other. Such a superposition manifests itself by emergent peaks. The peaks near the slits seem short. And they become longer, as a look moves from the slits to the far-field region. As soon as

the detector is shifted to the far-field region, the peaks are transformed to typical diffraction rays going away to infinity.

IV. DENSITY DISTRIBUTION PLOT AND BOHMIAN TRAJECTORIES.

Let us project the density distribution $p(x, z)$ to the plane (x, z) . Fig. 7 demonstrates this projection in grey palette. Dark places show maximal values of $p(x, z)$, black patches, in particular, side with the slits. Light places relate to minimal values. Fractality in the interference pattern are well visible when passing from the slit sources to the right edge of the figure.

Violet curves traced in the upper part of the figure depict bohmian trajectories. Finding the trajectories is based on variation of the action integral [17], which leads to the principle of least action. A general formula computing the bohmian trajectory [13, 18], the guidance equation [19, 20], reads:

$$v_x = \dot{x} = \frac{\hbar}{m} \Im \left(|\Psi(x, z)\rangle^{-1} \nabla |\Psi(x, z)\rangle \right) \quad (15)$$

As a result, we can find a current position of the particle by the following formulas:

$$\begin{cases} x(t) = x_0 + \int_0^t v_x d\tau, \\ z(t) = z_0 + v_z \cdot t. \end{cases} \quad (16)$$

The velocity along z is $v_z = \hbar k_z / m$. It stems from the term $\exp i\omega t - \mathbf{i}k_z z$ as adopted before, see Eq. (9).

Velocity v_x is seen from Eq. (15) to be (a) proportional to gradient of the wave function; and (b) inversely proportional to the same wave function. It means: (a) a trajectory undergoes greatest variations in parts, where the wave function demonstrates slopes; and (b) the trajectory avoids areas, where the wave function tends to zero. Violet wavy curves in Fig. 7 manifest themselves the above properties well enough. One can see, the wavy curves group predominantly in dark-grey spots and avoid white spots. In extreme cases, the trajectories traverse the white spots almost transversally.

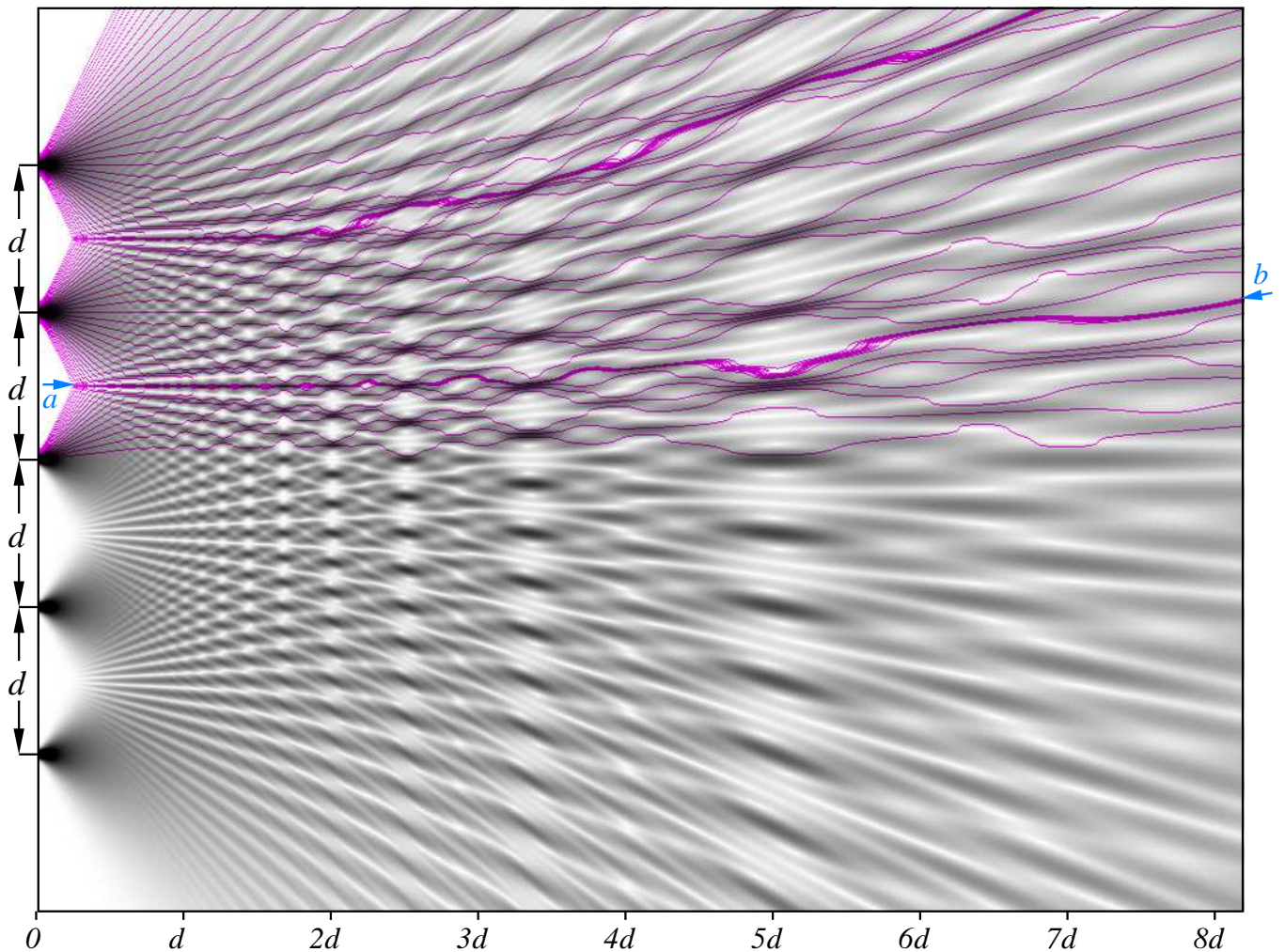


FIG. 7: Density distribution plot drawn by grey palette displays the Talbot effect: white color relates to zero intensity, and black color points to maximal intensity. Violet curves drawn in the upper part of the plot depict the bohmian trajectories. Distance $d = 5 \times 10^{-8}$ m. It is equal to $10 \cdot \lambda$, $\lambda = 5 \times 10^{-9}$ m..

Does this bohmian trajectory pattern relate to the many-worlds theory? Answer is negative [19, 21]. For that aim, let us scatter particles on the N -slit grating by single-piece. Let a single particle pass, for example, the central slit nearby the top border. As is shown in Fig. 7, the particle scatters to a direction pointed out by blue arrow a . Next, the particle goes on a wavy stream and follows to a place pointed out by blue arrow b . Here we suppose that, movement of the particle submits to the principle of least action. Therefore, a number of problems arises right now. The first problem arising here is as follows: what is cause which forces the particle to change its own direction in the vicinity of point a ? And the

second problem is: what is cause which forces the particle to perform wavy motions? We confirm that, any experimental setup for a quantum mechanical experiment is, in fact, the quantum instrument. The setup contains, in our case, N -slit grating with its parameters fitted for a wavelength of the particle. Boundary conditions of the setup determine the wave function on the edges. In whole, the experimental setup determines configuration of the wave function given in the working space. The function is named de Broglie pilot-wave [19, 20]. In fact, its squared image, the density distribution (11), is shown in Fig. 7 in grey palette. So, the bohmian trajectory shows an optimal path for a particle, which

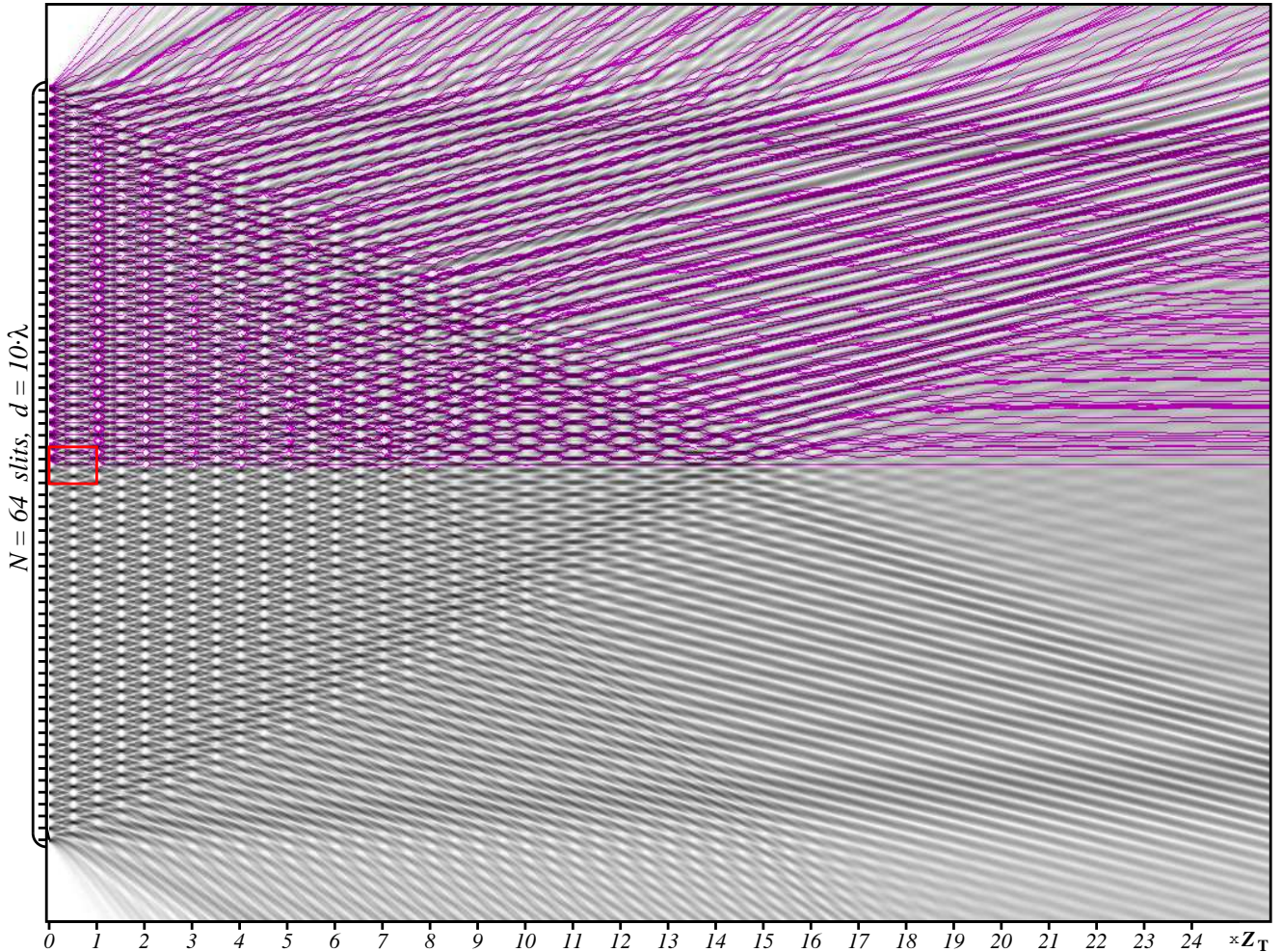


FIG. 8: Interference from $N = 64$ slits in the near-field region. Density distribution plot drawn by grey palette displays the Talbot effect: white color relates to zero intensity, and black color points to maximal intensity. Violet curves drawn in the upper part of the plot depict the bohmian trajectories. Grating parameters are $\lambda = 5$ nm, $d = 10\lambda = 50$ nm, $z_T = 1000$ nm.

is guided by the de Broglie pilot-wave within the working space.

V. FRACTALS IN THE NEAR-FIELD REGION.

In order to study fractal patterns arising in the near-field region in detail, amount of slits in the grating is not enough. In fact, the amount should tend to infinity. We will consider here, however, emission from a finite grating containing 64 slits, see Fig. 8. One can see, in the vicinity of the slits placed in the middle of the grating (in the figure that place is drawn by red square)

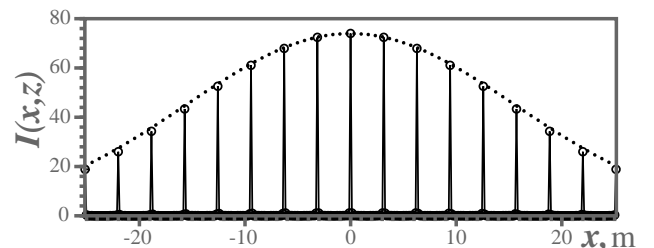


FIG. 9: Diffraction in the far-field region, $z = 1.25$ m. Cross-section of the diffraction pattern is displayed by circles. Solid sharp principal peaks show the same cross-section calculated by the diffraction formula (2) with parameters ζ and I_0 defined in Eqs. (12) and (13). Dot envelope curve is $I_0(x) \cdot N^2$.

the Talbot carpets can be perfect enough. As the wave front spreads to an area reaching to

the far-field region, the Talbot ordered structure is dissolved by triangle-like manner, as is described in [12]. In the far-field region we will observe an usual diffraction from N -slits, i.e., a set of principal maxima partitioned from each other by $(N - 2)$ subsidiary maxima, Fig. 9.

Violet wavy curves drawn in the upper part in Fig. 8 are Bohmian trajectories. They occupy preferably regions, where the probability density reaches local maxima. And vice-versa, they avoid local minima. Instructive to compare behavior of these Bohmian trajectories with those shown in Sanz's and Milét's article [12].

A. Talbot carpets.

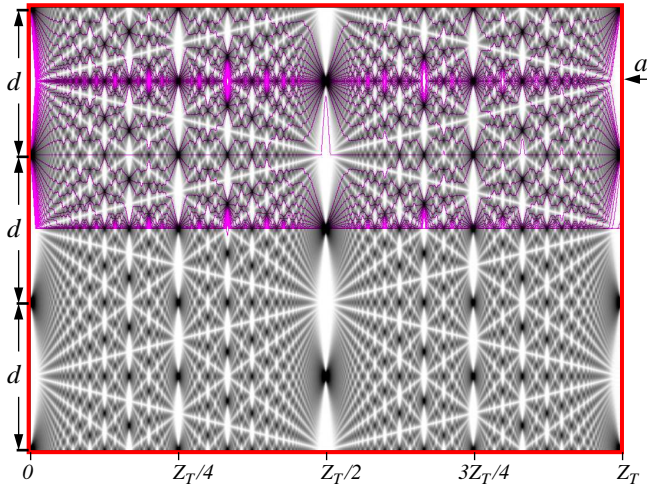


FIG. 10: Talbot carpet: $d = 10\lambda = 50$ nm, $z_T = 1000$ nm.

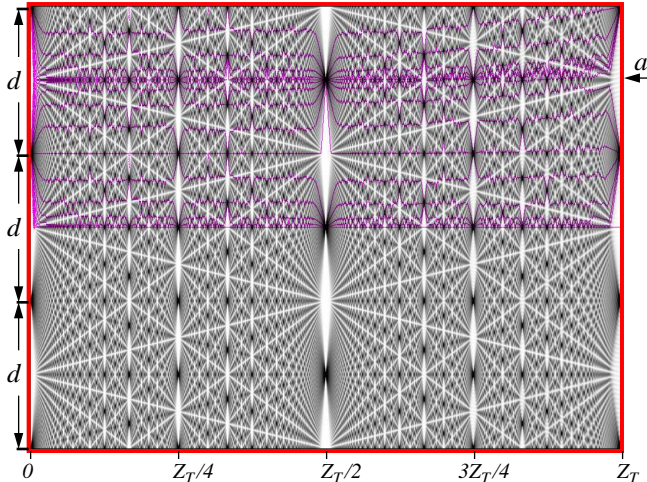


FIG. 11: Talbot carpet: $d = 20\lambda = 100$ nm, $z_T = 4000$ nm.

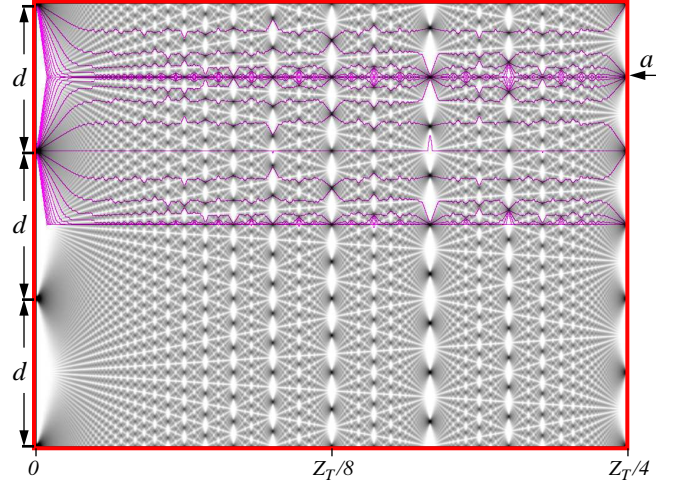


FIG. 12: Talbot carpet: $d = 40\lambda = 200$ nm, $z_T = 16000$ nm.

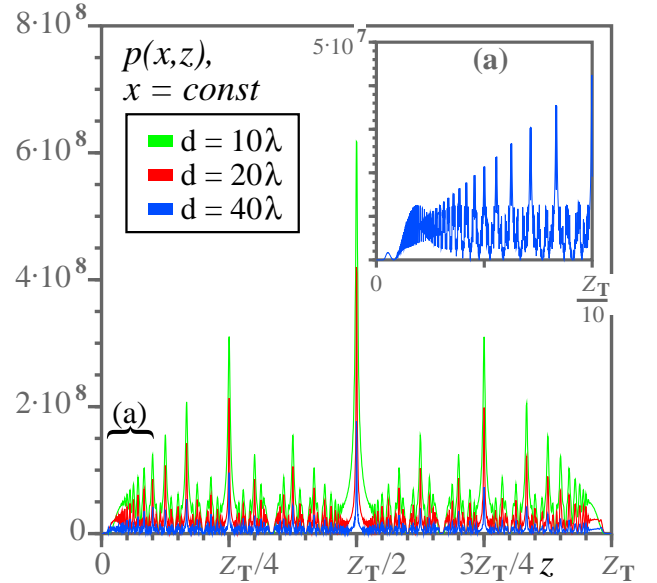


FIG. 13: Probability density distributions along cross-section pointed out by arrow a in Figs. 10, 11, and 12 are shown by green, red, and blue colors, respectively. Insert (a) shows behavior of $p(x, z)$ near the origin of coordinates.

Let us now discuss the Talbot patterns cut from the red square adjoining to the slit screen, see Fig. 8. Here we study emergence of the Talbot carpets at different relations of the period d and wavelength λ . Since the slit grating contains only $N = 64$ slits, we can study a small set of such relations, $d = k\lambda$, k is integer. We have given $d = 10\lambda$, $d = 20\lambda$, and $d = 40\lambda$. According to Eq. (1), we have $z_T = 2kd$. In the Talbot's units we can compare the Talbot carpets calculated for different input parameters. Figs. 10, 11, and 12 demonstrate the Talbot carpets calcu-

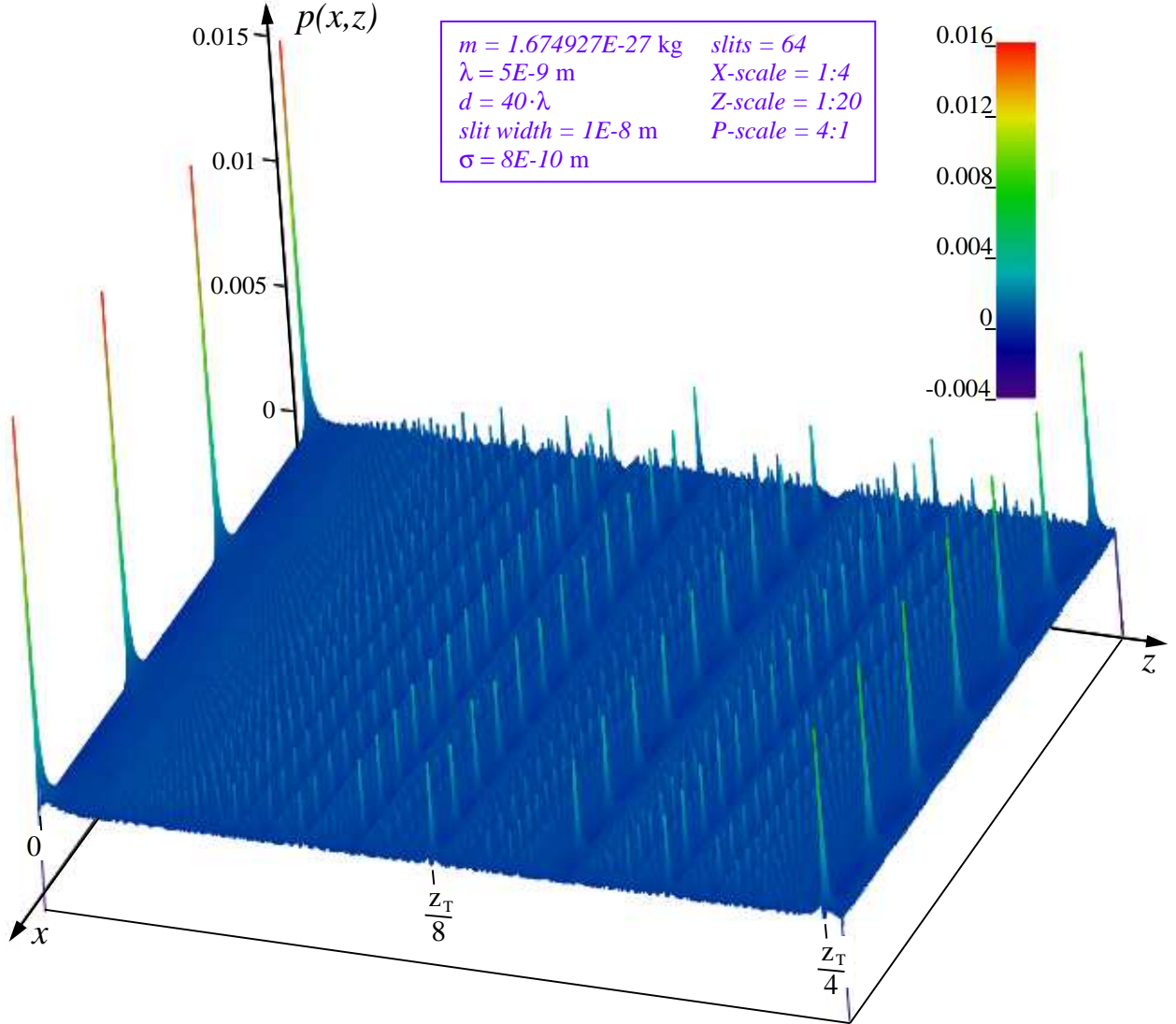


FIG. 14: Probability density distribution approaches infinite set of δ -functions as λ/d tends to zero.

lated at $\lambda = 5$ nm and $d = 10\lambda = 50$ nm, $d = 20\lambda = 100$ nm, $d = 40\lambda = 200$ nm, respectively.

Instructive to compare Talbot carpets shown in Figs. 1 and 10. The both figures are seen to relate to each other as negative and positive images. One can see, the both carpets show equivalent details. Whereas, the Talbot carpet shown in Fig. 11 is seen to contain more subtle details. In other words, this carpet is more fine-grained, than previous one. The Talbot carpet shown in Fig. 12 contains so much subtle details that the figure has been drawn only in the first quarter of the Talbot Length z_T . Here we can see fractal organization of the Talbot carpet very clearly.

Behind the N -slit grating, the field we can

see in Figs. 10, 11, and 12 has a fractal structure of fantastic complexity. Let us glance on behavior of the probability density distribution along a cross-section pointed out by arrow a in these Figs. We see, that the probability density vanishes at points $z = 0$ and $z = z_T$ and it reaches maximal values at $z = z_T/4$, $z = z_T/2$, $z = 3z_T/4$. In the other points the probability density alternates minimal and maximal values by irregular manner. More strictly, the irregularity exposes fractal nature. Fig. 13 shows behavior of the probability density distribution along the mentioned cross-section. Insert (a) shows its behavior near the origin of coordinates, $z \in (0, z_T/10)$. One can guess, that the probability density distribution tends to Cantor-like

set, as d/λ tends to infinity. This is in good agreement with a statement given by Berry *et al.* in [4], that proclaims that the Talbot fractal emerges as the ratio λ/d approaches zero and when the number N of illuminated slits tends to infinity as well [2, 3]. At N finite, however, the Talbot patterns are blurring and defocusing. And what is more, the Talbot effect is destroyed catastrophically as an observer shifts the detector either to edge of the N -slit grating or beyond the near-field region.

The Cantor set is a set of points lying on a single line segment that has a number of remarkable and deep properties [34]. First, the Cantor set cannot contain any interval of non-zero length. On the other hand, integral of the probability density distribution throughout all physical space has to be equal to unit. From here it follows, that the probability density distribution approaches an infinite set of δ -functions, see Fig. 14, as the ratio λ/d tends to zero.

Physically, limit of $\lambda \rightarrow 0$ is not available. It should be noted here, that at the wavelength tending to zero, kinetic energy of the incident particles approaches infinity. In that case, the particle beam will heat up the grating. And secondly, if the kinetic energy is increased further, the particles begin to destroy the grating.

In the upper parts of Figs. 10, 11, and 12, Bohmian trajectories representing particle's paths have been drawn. They are pictured by violet dots tracking predominantly along dark places relating to heightened values of the probability density. Their behavior is well visible in the vicinity of the dark nodes localized at cross-sections $z_T/4$, $z_T/2$, $3z_T/4$. In general, particles jump along separated points until they leave the near-field region. Real possibility is that, the particle is tunneling throughout the suppressed intervals. In other words, it reaches the far-field region along fantastical zigzag paths, that are frequently interrupted by tunneling. One can see, behavior of the Bohmian trajectories is complex enough in the fractal media. Nevertheless, it is predictable, since it is based on solution of two coupled equations - the quantum Hamilton-Jacobi equation and the continuity equation. The both result from the Schrödinger equation.

VI. CONCLUDING DISCUSSION.

A fractal, as defined by Mandelbrot, "is a shape made of parts similar to the whole in some way" [22]. An exact fractal is an "object which appears self-similar under varying degrees of magnification in effect, possessing symmetry across scale, with each small part replicating the structure of the whole" [22]. In this key Berry has also written in a private communication the following assertion "Fractality requires three conditions: infinitely many slits, paraxial propagation, and discontinuous initial conditions (i.e. sharp slits). Then the fractal structure, including fractal dimensions, can be calculated explicitly." As for the fractal Talbot effect, Berry *et al.* have written in [4] "Quantum and optical carpets provide a dramatic illustration of how limits in physics that seem familiar can in fact be complicated and subtle. It is no exaggeration to say that perfect Talbot images, and infinite detail in the Talbot fractals, are emergent phenomena: they emerge in the paraxial limit as λ/d (here d is signed instead of a , V. S.) approaches zero. At first this seems paradoxical, because the short-wave approximation is usually regarded as one in which interference can be neglected, whereas the Talbot effect depends entirely on interference. The paradox is dissolved by noting that the Talbot distance increases as the wavelength approaches zero, so here we are dealing with the combined limit of short wavelength and long propagation distance: in the short-wavelength limit, the Talbot reconstructed images recede to infinity."

Talbot patterns arising in the near-field region demonstrate the above mentioned signs fully. These patterns have emergent at simulation of scattering cold neutrons on many-slit grating (we have chosen parameters relating to this particle). A question arises here - how does a single particle travel behind the grating?

First of all, let us recall some solutions from the classical mechanics [23].

Geodesic trajectories in classical mechanics to be found by applying the principle of least action [23] are real trajectories of mechanical objects. A beam of the trajectories, that tracks a

relief, stems from the initial conditions slightly differing from each other. Observe that the geodesic trajectories nowhere never intersect.

The number of trajectories, crossing a surface δS , is conserved, no matter how the surface deforms at moving along the beam. In fact, this observation demonstrates the conservation law of number of the trajectories passing through the surface, i.e., the trajectories never disappear and does not appear again. Violation of this law in classical physics would be tantamount to recognize teleportation - a classic body disappear suddenly and unexpectedly announced again.

Interpretation of the continuity equation of the density of trajectories is guided by incompressible fluid, which flows along routes specified by the geodesic trajectories. All physical space we can imagine is filled with this fluid [23, 24]. The basis for such an idealization is experience which shows, that there is a rather broad class of fluids for which even large changes in pressure do not lead to significant change in density. This fluid fills the environment continuously. Its molecular structure, at that, is ignored. In classical physics the continuity equation does not determine the fate of trajectories in the future. Their fate is determined only by the Hamilton-Jacobi equation. Other situation arises in quantum mechanics. Here the both equations, the continuity equation and the Hamilton-Jacobi equation, connected with each other via the bohmian quantum potential [14, 15], take part in determination of the geodesic trajectories. First scientist was Madelung who had derived the same set of equations in 1926 [25].

In accordance with the de Broglie-Bohm interpretation, the wave function sets up a Ψ -field, which fills physical space of the experimental setup. Its squared modulus, the probability density distribution, is shown in Figs. 7,8,10–12, in gray palette. All physical space we can guess is filled by a fluid-like background with the density distribution $|\Psi|^2$ [25, 26]. It is important to note, that the state of such a fluid is determined by geometry of the experimental setup. And route of the trajectories depends on the density of the fluid, its gradients, in the neighborhood of each

point of the experimental setup. The guidance equation allows to find the trajectories that penetrate the field by the best way. In turn, the density distribution depends on the route of the trajectories. They are mutually dependent.

Such a fluid is seen to be vacuum. Polarization of vacuum is an extraordinary phenomenon since Hendrik Kasimir had proposed the existence of physical forces arising from a quantized field [27]. From this perspective, change of direction of a trajectory of a particle can be expressed in terms of exchange of virtual particles in vacuum. The vacuum has a vastly rich structure. It, implicitly, has all of the properties that a particle may have. This situation can be expressed by a sentence - the vacuum contains relative '*nothing*', and at the same time, the potential '*all*'.

The Feynman path integral [28] is a way to understand many manifestations of the vacuum. In fact, a proposition is as follows: virtual pairs emergent in a short time and annihilating in the end of the time loop are pairs permitting the particle to test a trajectory both forward and backward in time [29, 30, 31]. The extra degree of freedom obtained by allowing both directions in time gives the particle to get a non-local information needed for establishing an optimal path from a source to detector without the involvement of intelligent particles, intelligent observers, or multiple universes.

Acknowledgments

The author thanks Dr. A. S. Sanz, who impelled more deep study of fractal interference patterns in the near-field region. The author thanks also Prof. M. V. Berry for valuable comments relating to the fractal Talbot effect. The author expresses his sincere thanks to Miss Pipa, the site administrator of Russian Quantum Portal, for developing and writing a program calculating the density distribution of the wave function at scattering particles on N -slit grating. The program draws also Bohmian trajectories outgoing from the slits.

-
- [1] A. D. Cronin, J. Schmiedmayer and D. E. Pritchard. Atom Interferometers, e-print URL <http://arxiv.org/abs/0712.3703v1>, (21 Dec 2007).
- [2] M. V. Berry and S. Klein. Integer, fractional and fractal Talbot effects, JOURNAL OF MODERN OPTICS **43**(10) (1996) 2139-2164.
- [3] M. V. Berry. Quantum fractals in boxes, J. Phys. A: Math. Gen. **29** (1996) 66176629.
- [4] M. Berry, I. Marzoli, and W. Schleich. Quantum carpets, carpets of light, Phys. World (6) (2001) 1-6.
- [5] E. J. Amanatidis, D.E. Katsanos and S.N. Evangelou. Fractal Noise in Quantum Ballistic and Diffusive Lattice Systems, e-print URL <http://arxiv.org/abs/quant-ph/0310125>, (20 Oct 2003).
- [6] A. S. Sanz. A Bohmian approach to quantum fractals, J. Phys. A: Math. Gen. **38** (2005) 60376049.
- [7] J. F. Clauser and J. P. Dowling. Factoring integers with Young's N-slit interferometer, PHYSICAL REVIEW A **53**(6) (1996) 4587-4590.
- [8] A. Steane. Quantum Computing, Rept. Prog. Phys. **61** (1998) 117-173.
- [9] S. Olmschenk, D. N. Matsukevich, P. Maunz, D. Hayes, L.-M. Duan, and C. Monroe. Quantum Teleportation Between Distant Matter Qubits, e-print URL <http://arxiv.org/abs/0907.5240>, (30 Jul 2009).
- [10] V. I. Sbitnev. Particle scattering on a N-slit screen: Talbot carpet and far-field diffraction, Kvantovaja magija **6**(1) (2009) 1101-1112, in Russian.
- [11] M. M. Agamalyan, G. M. Drabkin, and V. I. Sbitnev. Spatial spin resonance of polarized neutrons. A tunable slow neutron filter, Phys. Rep. **168**(5) (1988) 265-303.
- [12] A. S. Sanz and S. Miret-Artés. A causal look into the quantum Talbot effect, J. Chem. Phys. **126** (2007) 234106; e-print URL <http://arxiv.org/abs/quant-ph/0702224>, (19 Jun 2007).
- [13] A. S. Sanz and S. Miret-Artés. A trajectory-based understanding of quantum interference, J. Phys. A: Math. Gen. **41** (2008) 435303; e-print URL <http://arxiv.org/abs/0806.2105>, (1 Oct 2008).
- [14] D. Bohm, A suggested interpretation of the quantum theory in terms of "Hidden Variables", Phys. Rev. **85** (1952) 166-193.
- [15] D. Bohm and B. J. Hiley. *The Undivided Universe: An ontological interpretation of quantum theory*, (Routledge, London, 1993).
- [16] G. I. Mark. Analysis of the spreading Gaussian wavepacket, Eur. J. Phys. **18** (1997) 247-250.
- [17] V. I. Sbitnev. Bohmian trajectories and the path integral paradigm. Complexified Lagrangian mechanics IJBC, **19**(7) (2009) xxxx-xxxx; e-print URL <http://arxiv.org/abs/0808.1245>, (8 Aug 2008).
- [18] M. Davidović, D. Arsenović, M. Božić, A. S. Sanz, and S. Miret-Artés. Should particle trajectories comply with the transverse momentum distribution?, Eur. Phys. J. Special Topics **160** (2008) 95, e-print URL <http://arxiv.org/abs/0803.2606>, (18 Mar 2008).
- [19] A. Valentini. De Broglie-Bohm Pilot-Wave Theory: Many Worlds in Denial? In: *Everett and his Critics*, eds. S. W. Saunders et al. (Oxford, University Press, 2009), e-print URL <http://arxiv.org/abs/0811.0810>, (5 Nov 2008).
- [20] W. Struyve and A. Valentini. de BroglieBohm guidance equations for arbitrary Hamiltonians. J. Phys. A: Math. Theor. **42** (2009) 035301 (18pp).
- [21] A. Kent. One world versus many: the inadequacy of Everettian accounts of evolution, probability, and scientific confirmation, In *Many Worlds? Everett, Quantum Theory and Reality*, eds. S. Saunders, J. Barrett, A. Kent and D. Wallace, O.U.P. upcoming, e-print URL <http://arxiv.org/abs/0905.0624>, (5 May 2009).
- [22] P. S. Addison, Fractals and Chaos (Institute of Physics, Bristol, 1997).
- [23] C. Lanczos. *The variational principles of mechanics*, (Dover Publ., Inc., N. Y. 1970).
- [24] R. E. Wyatt. Wyatt2005 *Quantum Dynamics with Trajectories: Introduction to Quantum Hydrodynamics*, (Springer, Berlin, 2005).
- [25] E. Madelung. Quantentheorie in Hydrodynamischer form. Zts. f. Phys, **40** (1926) 322 326.
- [26] D. Bohm and J. P. Vigier. Model of the Causal Interpretation of Quantum Theory in Terms of a Fluid with Irregular Fluctuations, Phys. Rev. **96**(1) (1954) 208 - 216.
- [27] H. G. B. Casimir. On the attraction between two perfectly conducting plates, Proc. Con. Ned. Akad. van Wetensch B51(7) (1948) 793-796.
- [28] R. P. Feynman and A. Hibbs. Quantum Mechanics and Path Integrals, (McGraw Hill, N. Y. 1965).
- [29] G. N. Ord and R. B. Mann. Entwined pairs and Schrödinger's equation, Annals of Physics, **308**(2003) 478-492; e-print URL <http://arxiv.org/abs/quant-ph/0206095>, (14 Jun 2002).
- [30] G. N. Ord, J. A. Gualtieri, and R. B. Mann. A physical basis for the phase in Feynman path integration, e-print URL <http://arxiv.org/abs/quant-ph/0411005>, (31 Oct 2004).
- [31] P. J. Werbos and L. Dolmatova. The Backwards-Time Interpretation of Quantum Mechanics - Revisited With Experiment, e-print URL <http://arXiv.org/abs/quant-ph/0008036>, (7 Aug 2000).
- [32] http://en.wikipedia.org/wiki/Talbot_effect
- [33] http://en.wikipedia.org/wiki/Thermal_neutron
- [34] http://en.wikipedia.org/wiki/Cantor_set